PHYSICS AND CHEMISTRY OF SOLID STATE
V. 26, No. 4 (2025) pp. 794-801
Section: Technology

DOI: 10.15330/pcss.26.4.794-801

Vasyl Stefanyk Carpathian National University

ФІЗИКА І ХІМІЯ ТВЕРДОГО ТІЛА
Т. 26, № 4 (2025) С. 794-801
Технічні науки

UDC: 621.774.21:669.14; 629.76/.78:620.1

ISSN 1729-4428 (Print)
ISSN 2309-8589 (Online)

L.I. Nyrkova, L.V. Goncharenko, Yu.I. Lisovskiy, L.I. Faynberg

Resistance against mechanical and corrosion-mechanical failure of welded joint of X70 steel with advanced viscous properties

E.O. Paton Electric Welding Institute of the National Academy of Sciences of Ukraine, Kyiv, Ukraine, lnyrkova@gmail.com

An arc welding method under flux for the controllable rolling of X70 steel for main gas pipelines, which improves the viscosity of the welded joint and resistance against stress-corrosion cracking (SCC) under cathode protection, was developed. The impact toughness of the weld at temperatures minus 40°C was KCV^{-40} = 189.0 J/cm^2 versus KCV^{-40} = 117.1 J/cm^2 for the base metal. The corrosion rates and electrochemical properties of different zones of the welded joint were determined, and their stress-corrosion cracking susceptibility in the NS4 medium was investigated using voltammetry, the slow strain rate method, and scanning electron microscopy.

Keywords: X70 steel, welded joint, slow strain tests, masometry, voltammetry, optical microscopy, scanning electron microscopy, corrosion, stress-corrosion cracking.

Received 07 October 2024; Accepted 30 October 2025.

Introduction

Pipeline transport is the main mode of transportation for oil and gas in the modern world, and its safety and reliability have an important impact on the smooth development of the regional economy, and even on the security situation. Many studies have investigated the factors of stress-corrosion cracking of high- and medium-strength tubular steels in soil or groundwater. Stress-corrosion cracking of pipeline steel in the soil during operation is a major hidden cause of danger. Depending on the composition of the external environment, stress-corrosion cracking of pipe steels mainly occurs according to one of two types: at high pH and at pH close to neutral. The susceptibility of steel to stress-corrosion cracking depends on the chemical composition of the corrosion environment and steel microstructure. Tubular steel with bainite or acicular ferrite grains is more inclined to stress-corrosion cracking in various solutions [1]. The applied load, stress concentration, and their fluctuations contributed to the initiation and development of stress-corrosion cracking. Generally, the crack initiation and propagation mechanisms in solutions with a pH close to neutral are anodic dissolution and hydrogen embrittlement [1-4].

In simulated groundwater, the susceptibility to stress-corrosion cracking in the heat-affected zone of a welded joint made of API X70 steel depends on two factors: the influence of the microstructure of this zone on electrochemical reactions and the influence of mechanical properties on the development of stress-corrosion cracking [5]. The microstructure in the heat-affected zone is soft, which can significantly facilitate the process of hydrogen release when the cathode potential is more positive than -1050 mV (relative to SCE). However, at potentials negatively than -1050 mV, the cathodic current densities on different microstructures are close in value, which is consistent with the electrochemical results: at potentials more negative than -650 and -850 mV, stress-corrosion cracking is most likely to occur in the zone with a soft structure, and from more negative than -1200 mV – in both soft and hard zones.

The electrochemical corrosion mechanism of a welded joint made of X70 steel in a near-neutral pH solution does not change during hydrogen permeation under the applied stress or under the influence of both factors [6]. Hydrogenation accelerates the local anodic dissolution of steel and reduces the stability of the

corrosion-product layer. The heat-affected zone exhibited the largest dissolution current after hydrogen penetration. An increase in stress increased the anodic dissolution rate of the welded joint in the heat-affected zone. A synergistic effect on the anodic dissolution of the welded joint made of X70 steel was observed when hydrogenation was performed with a current of 10 mA/cm^2 and a stress of 550 MPa. Under such conditions, the anodic dissolution of the welded joint increases by (5.7-6.5) times, maximally in the heat-affected zone.

In a welded joint made of X70 steel in an environment with a near-neutral pH, a stress corrosion crack can initiate from the microdimples on the surface of the heat-affected zone and propagate along the principal stress plane when the frequency of the load fluctuations increases to a certain degree [7], [8]. The crack propagates along the plane of maximum shear stress at an angle of 45 [8].

The preliminary plastic deformation of a welded joint made of X70 steel reduces the resistance to stress-corrosion cracking in the zones of this joint in a near-neutral pH solution [9]. Their susceptibility to stress-corrosion cracking can be arranged in the following order: heat-affected zone > weld metal > base metal. The fractographic analysis revealed the existence of two cracking modes. Type I cracks propagated perpendicular to the maximum tensile stress, whereas type II cracks were located in planes parallel to the plane of the maximum shear. Stress-corrosion cracking of the base metal and heat-affected zone occurs according to type I and the weld metal, mainly according to type II. The sensitivity to preliminary plastic deformation is a constant of the material, which makes it possible to propose this indicator for characterizing the susceptibility of sections to stress-corrosion cracking before they acquire preliminary plastic deformation. The increased susceptibility to stress-corrosion cracking caused by previous plastic deformation may be due to the increased yield strength. The correlation between the ratio of the reduction in the cross-sectional area of the NS4 solution to the area in air and the yield strength depended on the microstructure.

The experience gained at the EO Paton Electric Welding Institute showed that stress-corrosion cracking of the main gas pipelines spreads along the main metal at a distance of 25 mm from the fusion line with the seam [10], [11]. As a continuation of these studies, this investigation aimed to investigate the stress-corrosion cracking of a welded joint made of X70 steel, obtained by arc welding under a flux, in a solution with a pH close to neutral under cathodic polarization.

I. Experimental Details

This study was conducted on specimes of low-alloy ferrite-pearlite steel class X70 (yield strength 485 MPa, ultimate strength 590 MPa, and relative elongation no more than 20%) and a welded joint made with S3-MoTiB welding wire. One-sided control seams were welded on the A 909 M machine according to a V-shaped design with a size of 90°×4 mm. Welding was performed under an OK 10-74 flux using an S3-MoTiB wire. Welding mode: I = 850-890 A; U = 38 B; $V_{welding}$ = 25 m/h; V_{fs} = 110 m/h (welding wire feeding speed). The welded joint is shown in Figure 1, a. With the applied welding mode, satisfactory formation of the seam with a penetration of approximately 11 mm and reinforcement size of 22×4 mm was obtained (Figure 1, b).

The chemical composition of steel and weld metal is given in Table 1.

The mass fraction of elements in the weld metal was within the limits corresponding to the composition of the weld when the S3Mo-TiB wire was used for welding.

The impact toughness of the weld metal was determined according to a method described in [12]. The welded joint specimens were cut along the central part of the seam (perpendicular to the sheet plane). The temperature of the tests corresponded to the requirements established in the regulatory documents for the manufacture of pipes (minus 20°C) and for determining the margin of cold resistance of the weld metal at lower temperatures (minus 40° C).

Corrosion and corrosion-mechanical studies were carried out at room temperature in a solution of NS4 composition, g/l: 0.122 KCl + 0.483 $NaHCO_3$ + 0.181 $CaCl_2$ + 0.131 $MgSO_4$ [13]. Solutions were prepared in distilled water using reagents classified as "pure for analysis". The weight was measured using an analytical laboratory-scale VLR-200 instrument.

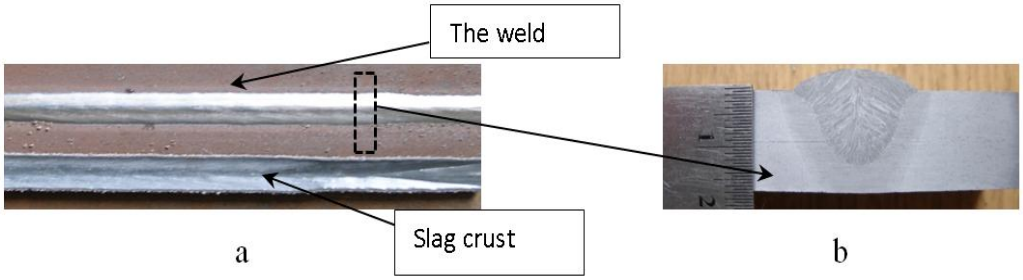

Fig. 1. Appearance of the welded joint template (a), obtained by single-arc welding of X70 steel under OK10.74 flux with S3MoTiB welding wire and macro grinding (b).

Table 1.

Chemical composition

Specimen characteristic	C	Mn	Si	S	P	Al	Ni	Mo	Ti	V	Nb	B
Steel X70	0.096	1.71	0.208	0.009	0.007	0.035	0.03	0.03	0.015	0.06	0.052	0.002
Weld	0.07	1.5	0.44	-	-	-	0.13	0.18	0.022	0.043	0.036	0.005

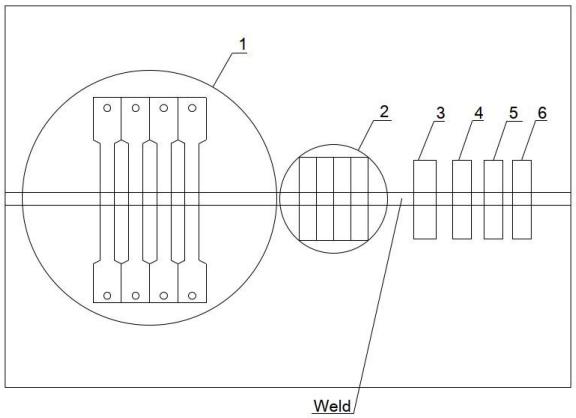

Fig. 2. Specimen cut-out scheme for various types of research: 1 – corrosion-mechanical; 2 – impact viscosity; 3 – metallographic; 4 – electrochemical; 5 – spectral analysis; 6 – electrolytic irrigation of steel; 7 – determination of corrosion rate.

The surfaces of the specimens were cleaned with sandpaper of different grain sizes, degreased with magnesium oxide, washed under running and distilled water, and dried with filter paper. A pressure cell was used to measure the potentials and polarization curves of the base metal and welded joint specimens.

The corrosion potentials were measured against a saturated silver chloride reference electrode (SSCE) for 1 h using an MTech PGP-550F potentiostat. Anodic and cathodic polarization curves were recorded for the base metal and weld seam of the welded joint specimens. The potentiodynamic mode and potential sweep speeds of 1, 0.5, and 100 mV/s were used.

Slow strain-rate tests were performed by deforming the specimens at a low rate of 10^{-6} s^{-1} on an AIMA-5-1 breaking machine in a corrosive environment. Specimens were prepared according to a previously described procedure (Figure 3). The reference and auxiliary electrodes were identical to those used in electrochemical experiments. The tests were carried out at cathode polarization potentials of -0.750 V, -0.950 V and -1.050 V (SSCE).

Specimens for metallographic studies were made according to the standard method, using diamond pastes of different dispersions. To examine the microstructure, the specimens were etched in nital (solution of 4% nitric acid in ethyl alcohol). Metallographic studies were performed on a NEOPHOT 21 microscope using an Allied Vision 1800 U-2050c digital camera and the SEO ImageLAB software. Grain scores were determined according to the DSTU ISO 643 [14]. The surfaces of the specimens after rupture were studied by scanning electron microscopy on a JSM 840 microscope (JEOL, Japan) in the mode of secondary backscattered electrons at an accelerating voltage of 20 kV and an electron beam current (10^{-7}-10^{-10}) A at magnifications of ×16, and ×500.

1.1. Microstructure

The microstructures of the base metal and the welded joints are shown in Figure 4. The microstructure of the base metal is typical of X70 steel, as described in detail in previous studies [10], [11]. The size of the ferrite grain was 11 μm [14], the amount of pearlite component was 12%, the banding was equal to to 4-5 points, and series B according to DSTU 8972 [15]. In the area of the large grains of the welded joint, the structure was of the bainite type (ferrite with second-phase discharges, mainly of lamellar morphology), and polygonal pre-eutectoid ferrite formed at the boundaries of the former austenite grains (Figure 4, b).

The average grain diameter in the overheating zone is

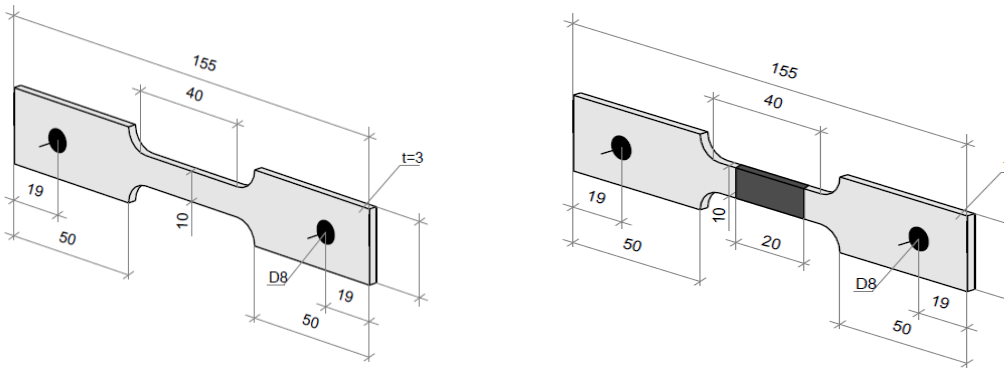

a b

Fig. 3. Sketches of specimens for slow strain rate tests.

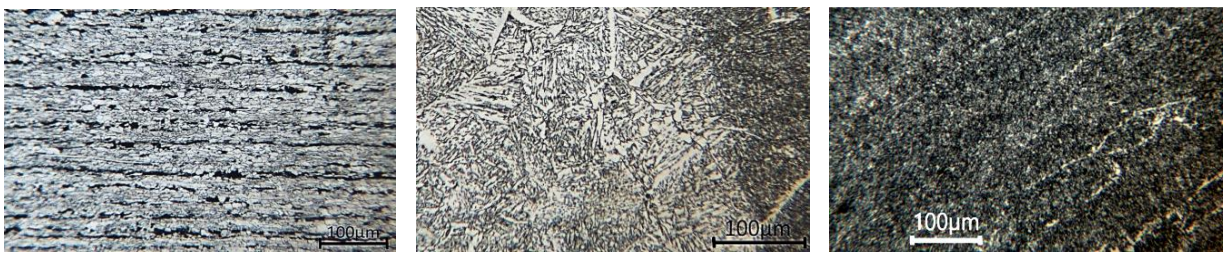

a b c

Fig. 4. Microstructure of the base metal of X70 steel and welded joint: a – base metal; b – heat-affected zone; c – weld.

(0.088-0.012) mm [15]. The length of the coarse grain zone of the examined welded joints ranged from 0.40 to 0.45 mm, and the length of the total zone of thermal influence was approximately 5.0 mm. In the structure of the seam, there are thinner intergranular layers of polygonal ferrite with widths of 5–7% with a width of (3-5) μm, which stand out at the secondary boundaries (Figure 4, c). These layers consist of ferrite grains, which are mainly discontinuous. The proportion of acicular ferrite is up to 80%, and the aspect ratio is 1:(2-10). Most acicular ferrites exhibit high angle boundaries. A grid of thin thread-like polygonal boundaries with the formation of the martensitic-austenitic crystallization phase was fixed on them (Figure 4, c).

From the analysis of the impact toughness test results, it was determined that the weld metal exceeded the impact toughness of the base metal at test temperatures of -20°C and -40°C.

As can be seen from Figure 5, a, c, macrofractures of specimens at temperatures of -20°C and -40°C have a viscous nature. The fiber direction preserved the visible traces of the structure of the cast seam. The seam has a rougher and more deformed surface. There were practically no flat (brittle) fragments on the fracture surface (Figure 5, b, d), and pits formed at the test temperatures of -20°C were smaller than at -40°C.

1.2. Electrochemical studies

The corrosion potentials of the X70 steel and weld in the NS4 solution were -0.661 mV and -0.658 V, respectively (Figure 6, a). The Tafel slopes of the anodic curves were 0.042 V, indicating diffusion control of the corrosion process (Figure 6, b). The limiting diffusion current of oxygen reduction on the weld was slightly lower than that on the X70 steel (0.156 A/m^2 and 0.178 A/m^2, respectively). This may indicate electrochemical heterogeneity between the weld and base metal. The delay in corrosion is presumably due to the difficulty of oxygen delivery to the corroding surface and removal of corrosion products.

The corrosion rate of X70 steel in the NS4 solution, weld metal, and heat-affected zone was 0.039, 0.024, and 0.039 mm/year, respectively.

1.3. Corrosion-mechanical research

The breaking curves of X70 steel and welded joints are shown in Figure 7. The rupture of the welded specimens (Figure 7, curves 2, 4, and Table 3) occurred at a lower relative elongation than that of the X70 steel, and the applying of cathodic polarization contributed to a change similar to that of the fracture (Figure 7, curves 3, 4).

For the specimens of both the X70 steel and the

Table 2.

Impact toughness

Characteristics of the specimens	KCV, J/cm ^{2} for temperatures	
	-15 °C/-20 °C	–40 °C
X70	128,3	117,1
Weld metal	188,0...196,2...203,2...208,9 199,1	174,1...189,4...194,9...197,5 189,0

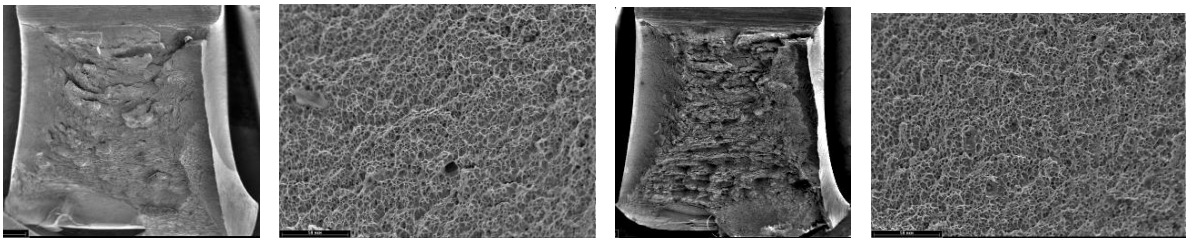

a b c d

Fig. 5. Typical character of the fracture surface of welded joint specimens with impact toughness values: a, b – KCV^{-20} = 208.9 J/cm^2; c, d – KCV^{-40} = 189.4 J/cm^2.

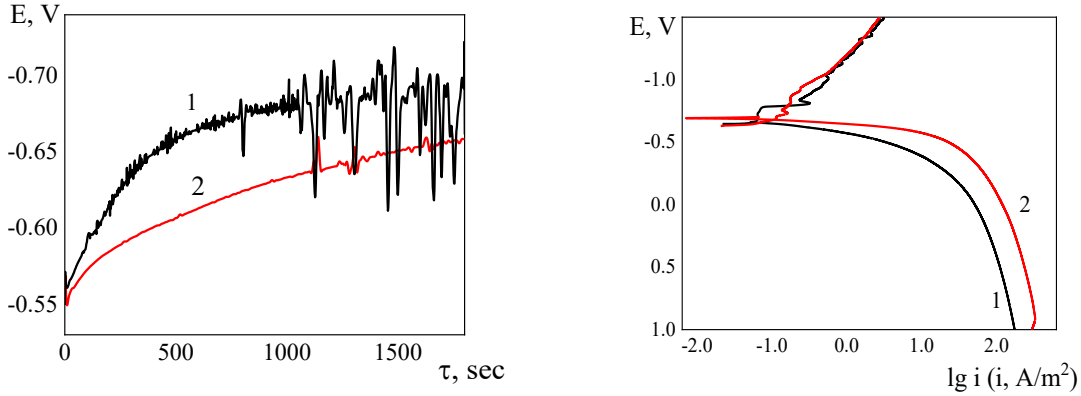

a b

Fig. 6. Changes in corrosion potentials (a) over time and polarization curves (b) of X70 steel (1) and the weld metal (2) in NS4.

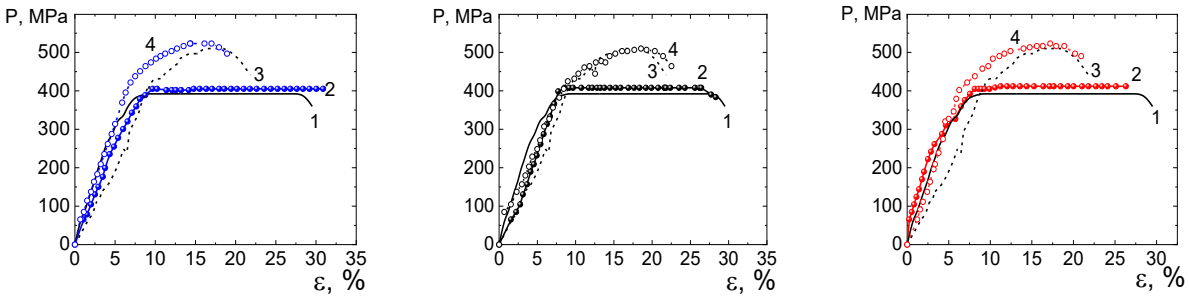

a b c

Fig. 7. Breaking curves of X70 steel (1, 2) and the welded joint made with S3Mo-TiB welding wire (3, 4) in air (1, 3), and in NS4 solution at polarization potentials (2,4): a – -0.750 V; b – -0.950 V; c– -1.050 V.

Table 3.

Mechanical properties of the welded joint of X70 steel and the welded joint in air and corrosion-mechanical properties in the NS4 solution at different polarization potentials

Test conditions, potential, V	τ_{break}, hours	σ_{US}, MPA	δ, %	S, mm^2	Ψ, %	K_s
Steel X70						
Air	43	390.52	29.52	8.09	73.02	-
-0.750	43	401.87	30.88	7.96	73.46	1.00
-0.950	42	413.06	28.31	10.41	65.30	1.12
-1.050	40	408.65	26.31	7.88	73.73	1.00
Welded jont made by S3Mo-TiB wire						
Air	35	510.35	21.81	8.42	71.94	-
-0.750	31	521.70	18.93	10.56	64.79	1.11
-0.950	32	510.35	23.50	12.75	57.49	1.25
-1.050	30	521.70	20.93	12.88	57.07	1.26

welded joint that ruptured in air, viscous failure was characteristic of the corresponding signs: narrowing of the metal near the place of rupture, and the presence of areas of plastic deformation (Figure 8).

The relative elongation of X70 steel was 29.52%, whereas that of the welded joint was 21.40% (27.5% less than that of the base metal). The relative narrowing of X70 steel was 73.02% (Table 3), and the relative narrowing after the rupture of the welded joint increased to 75.67% (by 3.6% compared to steel)

At a minimum protective potential of -0.750 V, shrinkage was present on the welded joint specimens, and the relative elongation after rupture was 18.93%. That is, in the NS4 solution at a minimum protective potential of -0.750 V, the relative elongation of the welded joint decreased by 38.7% compared with that of the base metal under the same conditions. The relative narrowing of the welded joint decreased to 64.79% (by 11.8% compared with that of the base metal), as shown in Table 3.

At a protective potential of -0.950 V on the specimens, the shrinkage near the rupture site was noticeably reduced (Figure 8). The relative elongation was 23.50%. That is, at the minimum protective potential of -0.950 V, the relative elongation of the welded joint was 17.0% less than that of the base metal (Table 3).

At the maximum protective potential of -1.050 V, the retraction near the rupture point in all specimens noticeably decreased (Figure 8). The relative elongation of the welded joint specimen was 19.74%. At a potential of -1.050 V, the relative elongation of the welded joint is 25.0% lower than that of the base metal (Table 3).

The coefficient of susceptibility to stress-corrosion cracking K_S (the ratio of the relative shrinkage of the specimens in the air to the relative shrinkage in the NS4 solution) in the solution as the protective potential increases in the range -0.750 B → -0.950 B → -1.050V for steel changes by 1.0 → 1.12 → 1.0, for the welded joint made with S3Mo-TiB wire, so 1.11 → 1.25 → 1.26. Consequently, an increase in the susceptibility of this welded joint to stress-corrosion cracking was observed compared with that of the parent metal.

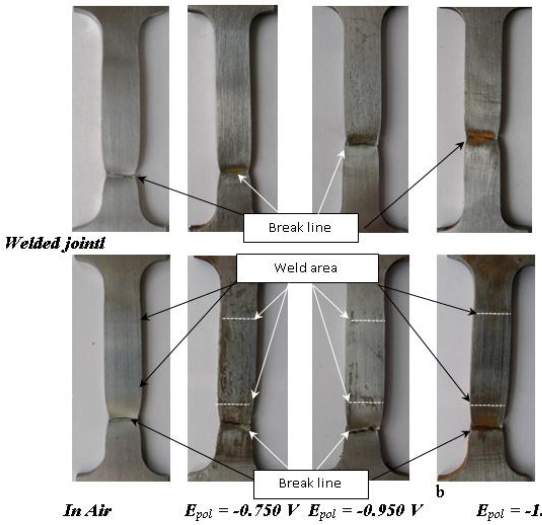

Fig. 8. View of the fracture area of X70 steel specimens (1) and welded joint (2) after slow strain rate tests in air (a) and in NS4 solution at protective potentials: b – -0.750 V; c – -0.950 V; d – -1.050 V.

For a more detailed analysis, a study of the fracture

surfaces of the specimens after the corrosion mechanical tests was conducted.

Notably, stress-corrosion cracking of the welded joint specimens occurred on the base metal under all test conditions, as shown in Figure 8. As noted in the study on the microstructures of the welded joint zones, the width of the thermally affected zone was 5.0 mm. In our opinion, this is quite natural, given the quality of the weld and its high-impact toughness. The welded specimens had a lower relative elongation because of the higher hardness of the weld metal; the welded specimens had a lower relative elongation.

1.4. Fracture studies

The fracture surface of X70 steel in air was formed as a result of the formation and destruction of small pores or after their union and destruction (Figure 9, a). Small inclusions were observed in some pits. Flat surface elements were formed by the destruction of pearlite bands.

After breaking of X70 steel at the minimum protective potential of -0.750 V, the structure of the fracture fragments differed slightly from the surface of the specimen tested in air. Larger viscous fragments were formed by the fusion and rupture of dimples; however, most of the fracture surface was formed by shear, owing to plastic deformation (Figure 9, c).

The fracture surface of the specimen of X70 steel after testing at a potential of -0.950 V also showed a viscous character; part of it was formed by the rupture of small pits, and the other, in the form of larger fragments, was formed by the union of small pits before rupture and rupture by non-metallic inclusions (Figure 9, e) The fracture surface of the specimens of X70 steel at a potential of -1.050 V is viscous, but less energy-intensive, and contains individual brittle fragments, possibly due to partial local hydrogen penetration due to cathodic polarization. A significant portion of the fragments at the edge of the specimen were formed by plastic deformation by shear and detachment. Several deep pits were recorded, apparently after the fallout of non-metallic inclusions, owing to the weakening of adhesion with the matrix (Figure 9, g).

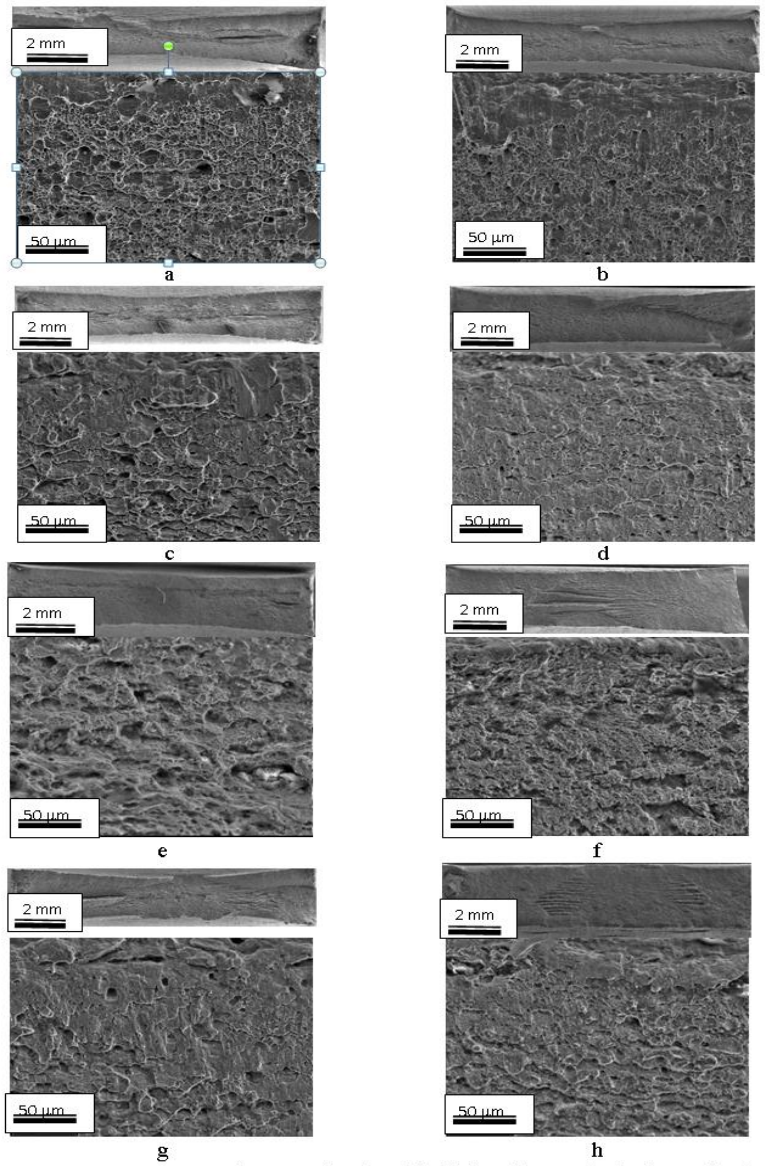

Fig. 9. Fractograms of X70 steel (a, c, e,g) and welded joint (b, d, f, h) after mechanical tests in air (a, b), corrosion-mechanical tests in NS4 solution at protective potentials: c, d – -0.750 V; e, f – -0.950 V; g, h – -1.050 V. × 16 (top photos), × 500 (bottom photos).

The fracture surface of the welded specimen in air shows that the fracture occurs due to plastic deformation by a viscous mechanism, during the formation and rupture of individual pores, and also after their union (Figure 9, b). The pits are mostly small, up to 5 μm in size. It is possible to distinguish some striation of the structure along the specimen, which is characterized by the presence of larger pits with a flat bottom. This fracture feature may be due to the destruction of the pearlite band in controlled rolling steel.

The destruction of the specimen at a potential of -0.750 V also occurred by a viscous mechanism during plastic shear deformation in the direction of specimen destruction and subsequent rupture (Figure 9, d).

The fracture surface of welded joint specimen of X70 steel, when tested at a potential of -0.950 V, consisted of most elements of a typical viscous nature, which were formed after the rupture of small dimples (Figure 9, f). Between these parts, there are deeper flat fragments that can be attributed to a quasi-brittle origin, possibly formed from the detachment of elements of the ferrite phase, or a harder fragment of the structure owing to plastic deformation. The cause of this specific structural weakening could also be the penetration of hydrogen into the metal surface of the specimen.

The fracture surface of the specimen at a potential of -1.050 V has signs of viscous fracture with small brittle fragments (Figure 9, h). Near the edge of the specimen, plastic deformation occurred mainly in the form of shear deformation, and the structure was a consequence of shear deformation and detachment, which led to the destruction of small pores and larger flat fragments formed by the union of small pores and dimples. Deeper local damage with a brittle diameter of approximately 45 μm of brittle nature due to intergranular destruction of the combined damaged grain with inclusions was observed close to the surface.

Conclusions

The corrosion, electrochemical, and corrosion-mechanical properties of an X70 steel welded joint made by single-arc welding under an OK 10-74 flux with S3MoTiB welding wire were investigated.

The rates of corrosion of the base metal from the X70 steel, weld seam, and thermally affected zone were 0.039, 0.024 mm/year0.039 mm/year

The corrosion potentials of the X70 steel and weld seam in the NS4 solution are -0.661 mV and -0.658 V, and the Tafel slopes of the anodic curves were equal to 0.042 V, indicating diffusion control of the corrosion process. The limiting diffusion current of oxygen reduction on the weld seam was slightly lower than that on the X70 steel, 0.156 A/m^2 and 0.178 A/m^2.

Stress-corrosion cracking of the welded joint in solution at polarization potentials of -0.75, -0.950 and -1.050 V occurred on the base metal, indicating the quality of the weld and its highly viscous properties.

Susceptibility to stress-corrosion cracking, estimated by the K_S coefficient in the NS4 solution) in the solution as the protective potential increases in the range -0.750 V → -0.950 V → -1.050 V for X70 steel changes such as 1.0 → 1.12 → 1.0, for the welded joint made with S3Mo-TiB wire – as 1.11 → 1.25 → 1.26. Consequently, an increase in the susceptibility of this welded joint to stress-corrosion cracking was observed compared with that of the parent metal.

Acknowledgments

This work was financially supported by the E.O. Paton Electric Welding Institute of the National Academy of Sciences of Ukraine (state registration number 0122U001188).

Nyrkova L.I. – Doctor of Engineering Sciences, Senior Researcher, Head of the Department of welding of gas and oil pipes
Goncharenko L.V. – Junior researcher of the Department of welding of gas and oil pipes
Lisovskiy Yu.I. – Postgraduated student of the Department of welding of gas and oil pipes
Faynberg L.I. – head of the group.

[1] S. A. Abubakar, S. Mori, J. Sumner, *A review of factors affecting SCC initiation and propagation in pipeline carbon steels*, Metals, 12(8), 1397 (2022); https://doi.org/10.3390/met12081397.
[2] S. Luo, R. Yuan, J. Wang, W. He, Y. Xue, M Liu, *Effect of Cathodic Polarization on SCC Behavior of a X52 Pipeline Steel in Service for 20 Years,* Journal of Materials Engineering and Performance, 1 (2023); https://doi.org/10.1007/s11665-023-09088-6.
[3] H. Yuan, Z. Liu, X. Li, C. Du, *Influence of applied potential on the stress corrosion behavior of X90 pipeline steel and its weld joint in simulated solution of near neutral soil environment*, Jinshu Xuebao/Acta Metallurgica Sinica, 53(7), 797 (2017); https://doi.org/10.11900/0412.1961.2016.00530.
[4] J. Luo, S. Luo, L. Li, L. Zhang, G. Wu, L. Zhu, *Stress corrosion cracking behavior of X90 pipeline steel and its weld joint at different applied potentials in near-neutral solutions,* Natural Gas Industry B, 6(2), 138 (2019); https://doi.org/10.1016/j.ngib.2018.08.002.
[5] Z. Y. Liu, C. W. Du, C. Li, F. M. Wang, X. G. Li, *Stress Corrosion Cracking of Welded API X70 Pipeline Steel in Simulated Underground Water*, J. of Materi Eng and Perform, 22, 2550 (2013); https://doi.org/10.1007/s11665-013-0575-2.
[6] G. A. Zhang, Y. F. Cheng, *Micro-electrochemical characterization of corrosion of welded X70 pipeline steel in near-neutral pH solution*. Corrosion Science, 51(8), 1714 (2009); https://doi.org/10.1016/j.corsci.2009.04.030.
[7] H. Wan, C. Du, Z. Liu, D. Song, X. Li, *The effect of hydrogen on stress corrosion behavior of X65 steel welded joint in simulated deep sea environment*. Ocean Engineering, 114, 216 (2016); https://doi.org/10.1016/j.oceaneng.2016.01.020.

[8] G. M. Omweg, G. S. Frankel, W. A. Bruce, J. E. Ramirez, G. Koch, *Performance of welded high-strength low-alloy steels in sour environments*, Corrosion, 59(7), 640 (2003); https://doi.org/10.5006/1.3277595.
[9] Lu B., JL. Luo, D.G. Ivey, *Near-Neutral pH Stress Corrosion Cracking Susceptibility of Plastically Prestrained X70 Steel Weldment,* Metall Mater Trans A, 41, 2538 (2010); https://doi.org/10.1007/s11661-010-0283-6.
[10] L. Nyrkova, A. Rybakov, L. Goncharenko, S. Osadchuk, Y. Kharchenko, *Analysis of the causes of fracture of the main gas pipeline,* Zaštita materijala, 64 (2), 177 (2023); https://doi.org/10.5937/zasmat2302177N.
[11] L. Nyrkova, P. Lisovyi, L. Gonchasrenko, S. Osadchuk, Y. Kharchenko, A. Klymenko, V. Kostin, *Investigation of stress-corrosion cracking of welded joint of H70 steel under cathodic polarization in near neutral environment,* Zaštita materijala, 64(1), 96 (2023); https://doi.org/10.5937/zasmat2301096N.
[12] National Standard of Ukraine EN 10045-1:2006 Materials metallic. Charpy impact test. Part 1. Test method (EN 10045-1:1990, IDT).
[13] de Sena R. Antunes, Bastos I. Napoleão, Plat G. Mendes, *Theoretical and Experimental Aspects of the Corrosivity of Simulated Soil Solutions, International Scholarly Research Notices*, Article ID 103715, 6 pages (2012). https://downloads.hindawi.com/archive/2012/103715.pdf.
[14] National Standard of Ukraine ISO 643:2009 (ISO 643:2003, IDT) Steels. Micrographic method determination of the apparent grain size.
[15] National Standard of Ukraine 8972:2019 Steel and alloys. Methods for detection and determination of grain size.

Л.І. Ниркова, Л.В. Гончаренко, Ю.І. Лісовський, Л.І. Файнберг

Опірність механічному та корозійно-механічному руйнуванню зварного з’єднання із підвищеними в'язкими властивостями зі сталі Х70

Інститут електрозварювання ім. Є.О. Патона Національної академії наук України, Київ, Україна, lnyrkova@gmail.com

Розроблено спосіб дугового зварювання під флюсом сталі Х70 контрольованої прокатки для магістральних газопроводів, який забезпечує підвищені в’язкі властивості зварного з’днання та тривкість проти корозійного розтріскування за катодного захисту. Ударна в’язкість зварного шва за температур мінус 40°С становила 189,0 Дж/см^2 проти 117,1 Дж/см^2 для основного металу. Визначено швидкість корозії та електрохімічні властивості різних зон зварного з’єднання, а також досліджено їх схильність до корозійного розтріскування в розчині NS4 методом деформації з малою швидкістю, вольтамперометрії, сканувальної електронної мікроскопії.

Ключові слова: сталь Х70, зварне з’єднання, випробування методом деформації з малою швидкістю, масометрія, вольтамперометрія, оптична мікроскопія, сканувальна електронна мікроскопія, корозія, корозійне розтріскування.